

Synthesis of Fe-C-N Hybrid via Direct Pyrolysis of EDTA Ferric Sodium as Effective Electrocatalyst for Oxygen Reduction Reaction

Xiang-Hui Yan^{1,*}, Ziwei Meng¹, Hao Xu¹, Tong Xue¹, Guoli Fang¹, Zhun Hu²

¹ School of Materials Science and Engineering, North Minzu University, Yinchuan 750021, China

² Institute of Industrial Catalysis, School of Chemical Engineering and Technology, Xi'an Jiaotong University, Xi'an 710049, China

*E-mail: yanxianghui@tsinghua.org.cn

Received: 1 November 2018 / Accepted: 18 April 2019 / Published: 10 June 2019

Fe-N-C materials are believed to have potential to replace expensive platinum-based catalysts for cathodic oxygen reduction reaction in fuel cells. Without any template or carbon support, iron and nitrogen co-doped Fe-N-C materials were prepared by direct pyrolysis of a single precursor containing C, N and Fe atoms from inorganic-organic EDTA ferric sodium. The obtained EDTAFeNa-HT2 with partial graphitization, mesopore size, large surface area, a degree of nitrogen doping and magnetism was electrochemically measured for oxygen reduction reaction (ORR) in 0.1 M KOH; the onset and half-wave potentials were 0.93 and 0.80 V, respectively, which were comparable to those of Pt/C catalyst. It was also found that acid-leaching could drastically enhance electrocatalytic activity and facilitated transferring the ORR process from two-electron to four-electron pathway. Furthermore, the second heat-treatment further improved ORR activity and maintained the four-electron pathway.

Keywords: Fe-N-C hybrid; Direct pyrolysis; EDTA ferric sodium; Electrocatalytic oxygen reduction; Acid-leaching

1. INTRODUCTION

Fuel cells have been generally regarded as one of environmentally friendly, highly efficient energy conversion technologies, however, dependence on expensive Pt-based catalysts used on the cathode in fuel cell still leave some obstacles for large-scale market applications. Recently, M-N-C (M = Fe, Co, etc.) materials have been developed into one of most effective non-precious metal oxygen reduction catalyst, which have potential to be a substitute for expensive platinum-based catalysts [1-6].

Generally, it was reported that M-N-C materials were prepared by heat-treating a mixture of

carbon supports, nitrogen-containing precursors and transition metal salts [7-14] or nanocasting method with sacrificial solid templates [15-18]. The interactions between the multi-precursors, however, are complicated and difficult to be controlled during the process of high-temperature pyrolysis [19-22]. Besides, the cost will accordingly rise with usage of more raw materials. If hard template such as mesoporous silica is employed to prepare Fe-N-C materials, the method will face challenges for industrial scale-up due to high cost and multiple-step operations. To compared with the employment of multi-components and complex technological steps, a direct pyrolysis or carbonization of a single precursor containing both carbon, nitrogen and iron atoms is believed to be more controllable and economical.

Herein we presented low-cost Fe-N-C material derived from direct pyrolysis of the sole EDTAFeNa, which was employed as carbon, nitrogen and iron precursor. The resulting Fe-N-C material was further modified by acid-leaching and subsequently a second heat treatment. Moreover, we studied type and content of Fe species, specific surface area, degree of graphitization and nitrogen-doping of these Fe-N-C materials obtained at different stages and their effects on electrocatalytic performances for ORR in alkaline electrolyte (0.1 M KOH). The Fe-N-C catalyst synthesized at the stage of a second treatment showed comparable activity and stability to conventional Pt/C (E-TEK, 20 wt% Pt). Acid-leaching is a key step for facilitating the transfer of ORR process from two-electron to four-electron pathway.

2. EXPERIMENTAL

2.1 Preparation of EDTAFeNa-derived samples

Fe-N-C materials were prepared by a direct pyrolysis process. Briefly, 2 g EDTAFeNa was added into a quartz boat and then placed in tube furnace. The sample was pyrolyzed from room temperature to 300 °C with a heating rate of 10 °C min⁻¹ and held for 1 h under flowing nitrogen, and then continue to be heated to 700 °C with a heating rate of 10 °C min⁻¹ and held for 2 h. After cooling, the powder was treated at 80 °C in 30 mL 0.5 M H₂SO₄ for a certain time under stirring. After filtrating, washing and drying, the sample was subjected to the second pyrolysis under 900 °C with a heating rate of 5 °C min⁻¹ and remained for 1 h. The resulting samples obtained at the stage of the first pyrolysis, acid-leaching and the second pyrolysis were denominated as EDTAFeNa-HT1, EDTAFeNa-AL and EDTAFeNa-HT2, respectively.

2.2 Physical characterization

The wide-angle X-ray powder diffraction (WAXRD) patterns were recorded on an XRD-6000 diffractometer using Cu K α radiation at 40 kV and 30 mA over the range 10~90°. N₂ adsorption-desorption isotherms were obtained at 77 K using a 3H-2000PS2 physisorption apparatus. Prior to the measurement, the samples were outgassed at 473 K under vacuum for 2 h. BET and BJH analysis were used to determine the surface area, pore volume and pore size distribution. The carbon structural analyses were carried out on a JY-HR800 Raman spectrometer using a 532 nm wavelength. Magnetic

measurements were performed on a vibrating sample magnetometer (VSM) of type MicroSenseEV9 at room temperature. Surface elementary composition was determined by ESCALAB220-IXL X-ray photoelectron spectroscopy (XPS).

2.3 Assessment of electrocatalytic performances for ORR

The electrocatalytic performances of EDTAFeNa-derived samples for ORR were evaluated in a three-electrode system at room temperature using a CHI630. A glassy carbon rotating disk electrode (GC-RDE, 0.19625 cm²), Ag/AgCl (3.5 M KCl) and a Pt wire were employed as the working, reference and counter electrodes, respectively. The each EDTAFeNa-derived catalyst ink was prepared according to the previous report [23]. Electrochemical measurement of the each catalyst was performed by coating 15 μ L of the catalyst ink onto the polished glassy carbon electrode.

3. RESULTS AND DISCUSSION

3.1 Characterizations

As shown in Figure 1a, the two diffraction peaks appearing at $2\theta = 26^\circ$ and 43.3° are assignable to the (002) and (101) diffractions of graphitic carbon, respectively [24]. The former is a typical indication of carbon structures such as graphitic or disordered carbon [25]. Obviously, the acid-leaching leads to an enhancement in the graphitic structure in the EDTAFeNa-AL but a negligible change is observed in the EDTAFeNa-HT2, as shown by the sharper peak. XRD analyses also reveal the presence of some iron entities including metallic Fe ($2\theta = 44.7^\circ, 65.0^\circ$ and 82.3°), Fe₃C ($2\theta = 37.6^\circ, 42.9^\circ$ and 43.7°) and Fe₃O₄ ($2\theta = 30.2^\circ, 35.6^\circ, 43.2^\circ, 53.7^\circ, 57.2^\circ$ and 62.8°) [23,26].

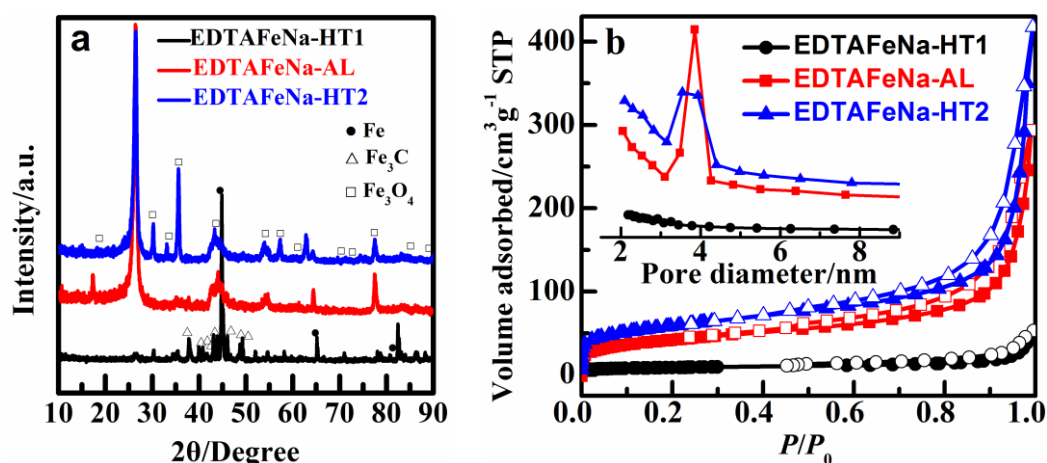


Figure 1. (a) XRD patterns and (b) N₂ adsorption/desorption isotherms and pore size distribution of EDTAFeNa-derived samples

From the pattern of EDTAFeNa-HT1, metallic Fe and Fe₃C are the predominant contributors to the Fe species. After acid-leaching (EDTAFeNa-AL), most of them have been removed and only weak

signals for Fe₃O₄ are observed. The diffractions for the EDTAFeNa-HT2 are in agreement with the those of EDTAFeNa-AL but appear to be higher peak intensity, which is maybe attributed to further oxidation of some Fe species and reduction of carbon mass during the second heat-treatment.

The porosity of EDTAFeNa-derived samples has been determined by nitrogen sorption analyses. From Figure 1b, all the isothermal curves exhibit type II with H3 hysteresis loops at a high relative pressure, which is an indicative of heterogeneous pores constructed from stack of sheet particles [27]; however, the curve of EDTAFeNa-HT1 shows a low uptake, signifying a low porosity. The pore size distribution curves disclose the presence of relatively uniform mesopores and micropores for both the EDTAFeNa-AL and EDTAFeNa-HT2. The textural parameters, listed in Table 1, show that EDTAFeNa-HT1 has very low pore volume and surface area, which is attributed to the existence of a mass of Fe species. Obviously, a large pore volume and surface area were obtained for EDTAFeNa-AL, suggesting that acid-leaching has removed most of Fe species and thus resulted in exposure of a large number of pores. After the second heat-treatment, the values of these parameters further increase, which could be explained by that carbon gasification led to formation of some extra pores.

Table 1. Textural properties of EDTAFeNa-derived samples

Sample	pore diameter (nm)	Pore volume (cm ³ ·g ⁻¹)	BET surface area (m ² ·g ⁻¹)
EDTAFeNa-HT1	3.9	0.08	52.5
EDTAFeNa-AL	3.9	0.46	248.2
EDTAFeNa-HT2	3.6	0.64	356.3

The carbon structural changes were investigated by Raman spectra (Figure 2a). The characteristic carbon peaks are found at around 1352 cm⁻¹ (D band) and 1582 cm⁻¹ (G band), respectively; the relative ratio of I_D and I_G is indicative of the overall order associated with the carbon structures; the larger the relative ratio is, the higher the overall disorder is [25,28]. The acid-leaching resulted in a decrease in disorder but the second heat-treatment led to a slight increase again. This is in accordance with the XRD analysis.

Field-dependent magnetization curves (Figure 2b) demonstrate that the EDTAFeNa-HT1 has a high saturation magnetization value (σ_s) of 69.3 emu/g, indicative of generation of an abundant of magnetic species. A dramatic decrease in σ_s can be observed for the EDTAFeNa-AL, which confirms that most of magnetic species such as metallic Fe and Fe₃C has been removed by acid-leaching. As for the EDTAFeNa-HT2, the σ_s only undergoes a slight of increase, which is mainly attributed to transformation of Fe species and a further carbon gasification during the heat-treatment.

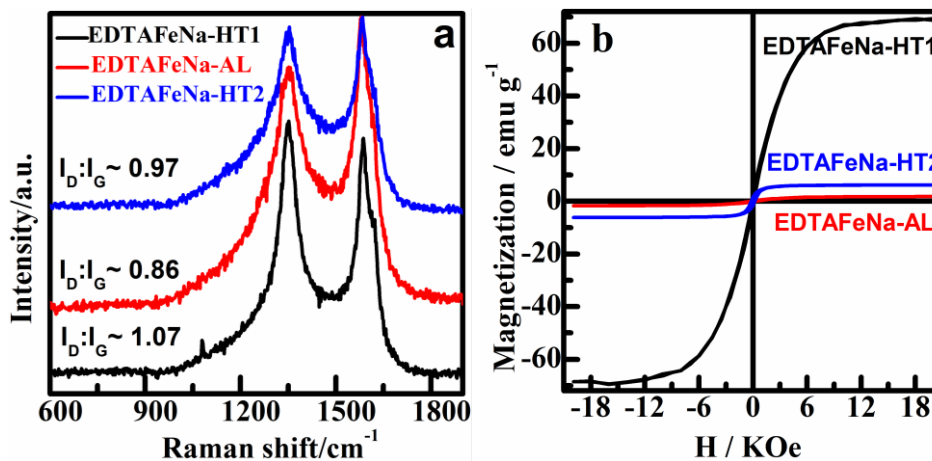


Figure 2. (a) Raman spectra and (b) field-dependent magnetization of EDTAFeNa-derived samples

The surface composition and chemical states of nitrogen species in the EDTAFeNa-derived samples were determined by XPS measurements. The survey spectra (Figure 3) show strong and distinct signals for C and O but weak signals for Fe and N in all samples.

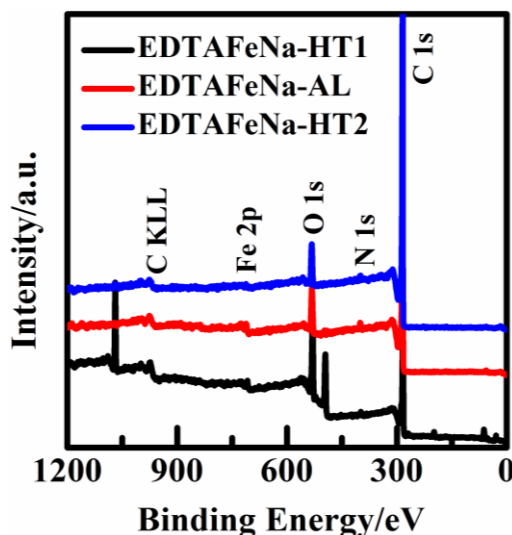


Figure 3. XPS spectra of EDTAFeNa-derived samples

Quantitatively (Table 2), although the total N contents in all these samples are low, nitrogen-doped carbon could be still obtained via a direct pyrolysis of the sole EDTAFeNa. The surface nitrogen content only declined slightly after acid-leaching and a second heat-treatment. To combine with the results of σ_s , the fairly low Fe content in all these samples indicated that most of Fe entities could be embedded in carbon matrices rather than distributed on the surface.

Table 2. Surface chemical composition and atomic concentration of the EDTAFeNa-derived samples

Sample	C	O	Fe	N
	at. %			
EDTAFeNa-HT1	78.29	19.21	0.71	1.79
EDTAFeNa-AL	89.96	7.79	0.70	1.56
EDTAFeNa-HT2	93.62	4.98	0.32	1.08

3.2 Electrocatalytic performance

The electrocatalytic performance of the EDTAFeNa-derived catalysts for ORR was investigated in an O₂-saturated alkaline electrolyte (0.1 M KOH) by a three electrode system using a rotating disk electrode (RDE). From the curves of linear sweep voltammetry (LSV) with a scan rate of 10 mV s⁻¹ and a rotation rate of 1600 rpm (Figure 4a), some parameters such as onset and half-wave potentials, and limiting current density could be obtained, which are listed in Table 3.

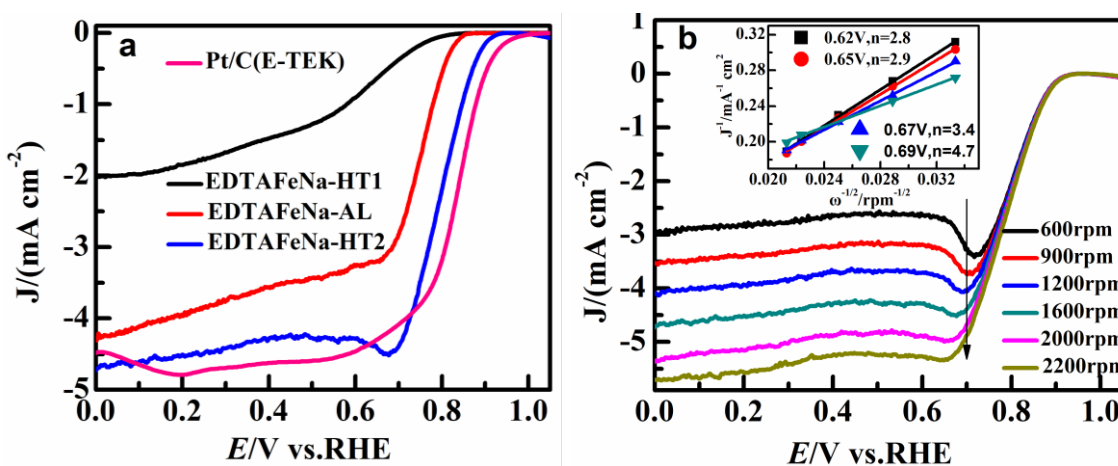


Figure 4. (a) Polarization curves of Pt/C and EDTAFeNa-derived catalysts in O₂-saturated 0.1 M KOH at a scan rate of 10 mV s⁻¹ and a rotation rate of 1600 rpm. (b) Polarization curves of the EDTAFeNa-HT2 at various rotation rates; the inset shows the corresponding K-L plots (J^{-1} vs. $\omega^{-1/2}$) at the indicated electrode potentials.

The data reveal that EDTAFeNa-HT1 shows a low activity for ORR, however, good activity relative to EDTAFeNa-HT1 is observed for EDTAFeNa-AL, with the ORR onset and half-wave potentials being notably high at 0.89 and 0.75 V vs. RHE, respectively. The ORR activity was further enhanced on EDTAFeNa-HT2; the onset and half-wave potentials are almost comparable to those of conventional Pt/C (E-TEK) catalyst. In retrospect of characterization data, a large amount of crystalline Fe species such as metallic Fe and Fe₃C was dispersed on the surface and encapsulated into carbon layers of EDTAFeNa-HT1. After acid-leaching, the mesopore remained unchanged (3.9 nm) but the σ_s and

surface area had a striking decrease and increase, respectively, which indicated the crystalline Fe species were first removed and generated abundant mesopores, presumably exposing more active sites. Thus, ORR activity was obviously improved on the EDTAFeNa-AL, which is in agreement with the previous reports [25,29-31]. After the second heat treatment, there were a further increase in surface area and higher disorder of carbon. Furthermore, the second heat treatment could repair the surface hydrophilicity of the catalyst by the acid-leaching step [25,30]. It is maybe attributed to that these factors exerted synergic effect on a further enhancement in ORR activity for the EDTAFeNa-HT2.

To make comparison, the ORR activity data are also summarized in Table 3 for some similar Fe-N-C electrocatalysts described in literature [28,32-38]. Recently, single-atom catalysts (SACs) have sparked intensive interests due to their excellent performance in electrocatalysis [39,40]. It can be seen that the highest activity was obtained for the Fe_{SA}-N-C and Fe-N_x ISAs/GHS with isolated Fe single atomic sites. The ORR activity exhibited by EDTAFeNa-HT2 in this work is at the moderate level among the values reported for various NPMCs (Table 3). However, it is anticipated that there is still a large room for improving the ORR activity of EDTAFeNa-derived Fe-N-C catalysts by optimization of preparations such as acid-leaching time, heat-treatment temperature and so on.

Table 3. ORR activity of the EDTAFeNa-derived catalysts in 0.1 M KOH and comparison with that of various Fe-N-C catalysts reported in literature*

Catalyst	E _{onset} (V)	E _{1/2} (V)	J _L (mA/cm ²)	Ref.	Catalyst	E _{onset} (V)	E _{1/2} (V)	J _L (mA/cm ²)	Ref.
EDTAFeNa-HT1	0.86	0.58	2.00	This work	Fe-N/C	0.91	0.79	4.63	[33]
EDTAFeNa-AL	0.89	0.75	3.48		Fe-A/P-CNT	0.93	0.73	7.47	[34]
EDTAFeNa-HT2	0.93	0.80	4.28		EFC	0.97	0.83	4.45	[35]
Pt/C (E-TEK, 20 wt% Pt)	0.99	0.83	4.60		Fe-N-C-800	0.91	0.73	3.82	[36]
EDC4	0.96	0.80	4.84	[28]	Fe _{SA} -N-C	1.02	0.89	6.00	[37]
NDG/Fe5.0	0.96	0.75	3.90	[32]	Fe-N _x ISAs/GHS	1.02	0.84	6.00	[38]

*E_{onset} and E_{1/2} were estimated from the polarization curves at 1600 rpm given in the literature. All potentials were given with respect to RHE, according to Nernst equation which is simplified to E (RHE) = E (Ag/AgCl) + 0.2046 V + 0.059 pH (pH = 13 for 0.1 M KOH).

The ORR mechanism on EDTAFeNa-derived catalysts in O₂-saturated 0.1 M KOH was further studied by LSV with varying the rotation rate from 600 to 2200 rpm, which were measured for estimating the number of transferred electrons (*n*) per O₂-reduction in the ORR process, according to the Koutecky-Levich (K-L) plot[41]. The LSVs for the EDTAFeNa-HT2, as a representative, were described in Figure 4b. The inset presents the corresponding K-L plots at selected electrode potentials (0.62 ~ 0.69 V); the slope of each K-L plot for all these catalysts were applied to calculate the values of number *n* at varied given potentials. The values of *n* for ORR on the EDTAFeNa-HT1 are ca. 2.0 while the values of *n* on the EDTAFeNa-AL increase to 2.8~4.0 in the whole potential range (not listed), which indicates that

ORR mechanism has changed due to acid-leaching. According to the values of n on the EDTAFeNa-HT2, it seems to be that the second heat-treatment has not altered the ORR mechanism. Although there has been a growing consensus that the FeN_x sites are the dominant active centers, recently, the iron and/or iron carbide encased in graphitic carbon layers (Fe-Fe₃C@C) have also been suggested as a new active site for Fe-N-C catalysts [42,43]. It was also revealed that Fe-N_x sites dominantly catalyse ORR via 4-electron pathway, serving as a major contributor to high ORR activity, whereas Fe-Fe₃C@C sites mainly promote 2e⁻ reduction of oxygen followed by 2e⁻ peroxide reduction, playing an auxiliary role[5,44,45]. To correlate ORR activity with their structural properties, it seems to be that the large specific surface area and more Fe-N_x sites exposed to mesopores are predominantly responsible for the high ORR activity of the EDTAFeNa-HT2 and carbon disorder is maybe also a positive factor based on the similar nitrogen content for the three catalysts.

4. CONCLUSIONS

In conclusion, the present EDTAFeNa-HT2 catalyst exhibited high ORR activity in alkaline electrolyte in terms of onset potential, half-wave potential and number of transferred electrons, which were nearly comparable to those of conventional Pt/C catalyst. It should be noted that a distinct improvement in catalytic performances for ORR is attributed to acid-leaching, which mainly function as to remove Fe species and accordingly increase specific surface area with more active sites exposed to mesopores. The activity further increased by the second heat-treatment, which mostly led to an increasement in specific surface area, carbon disorder and repair of surface hydrophilicity. These findings revealed that various Fe species contributed diversely but the meso-structure was at least a key factor for ORR activity. Therefore, to develop synergies by finely adjusting Fe species, pore size, specific surface area, carbon disorder and nitrogen content could still provide a big room for further enhancing the catalytic performance of EDTAFeNa-derived materials.

ACKNOWLEDGMENTS

This work was supported by the National Natural Science Foundation of China (No. 21563001), the Key Research Project of North Minzu University (No. 2015KJ20) and the Natural Science Foundation of Ningxia Province (No. NZ16091).

References

1. M. Lefevre, E. Proietti, F. Jaouen and J. P. Dodelet, *Science*, 324 (2009) 71.
2. G. Wu, K. L. More, C. M. Johnston and P. Zelenay, *Science*, 332 (2011) 443.
3. F. Jaouen, E. Proietti, M. Lefèvre, R. Chenitz, J. P. Dodelet, G. Wu, H. T. Chung, C. M. Johnston and P. Zelenay, *Energy Environ. Sci.*, 4 (2011) 114.
4. J. Tian, A. Morozan, M. T. Sougrati, M. Lefèvre, R. Chenitz, J. P. Dodelet, D. Jones and F. Jaouen, *Angew. Chem. Int. Ed.*, 52 (2013) 6867.
5. C. H. Choi, W. S. Choi, O. Kasian, A. K. Mechler, M. T. Sougrati, S. Brgller, K. Strickland, Q. Y. Jia, S. Mukerjee, K. J. J. Mayrhofer and F. Jaouen, *Angew. Chem. Int. Ed.*, 56 (2017) 8809.
6. Q. Ren, H. Wang, X. F. Lu, Y. X. Tong and G. R. Li, *Adv. Sci.*, 5 (2018) 1700515.
7. X. G. Li, G. Liu and B. N. Popov, *J. Power Sources*, 195 (2010) 6373.
8. K. X. Niu, B. P. Yang, J. F. Cui, J. T. Jin, X. G. Fu, Q. P. Zhao and J. Y. Zhang, *J. Power Sources*,

- 243 (2013) 65.
9. Q. Wang, Z. Y. Zhou, Y. J. Lai, Y. You, J. G. Liu, X. L. Wu, E. Terefe, C. Chen, L. Song, M. Rauf, N. Tian and S. G. Sun, *J. Am. Chem. Soc.*, 136 (2014) 10882.
 10. S. H. Tang, H. X. Huangfu, Z. Dai, L. P. Sui and Z. T. Zhu, *Int. J. Electrochem. Sci.*, 10 (2015) 7180.
 11. V. A. Setyowati, H. C. Huang, C. C. Liu and C. H. Wang, *Electrochim. Acta*, 211 (2016) 933.
 12. L. Osmieri, R. Escudero-Cid, M. Armandi, A. H. A. M. Videla, J. L. G. Fierro, P. Ocón and S. Specchia, *Appl. Catal. B: Environ.*, 205 (2017) 637.
 13. R. Wu, J. Wang, K. Chen, S. G. Chen, J. Li, Q. M. Wang, Y. Nie and Y. J. Song, *Electrochim. Acta*, 244 (2017) 47.
 14. T. T. Yang, M. Wang, X. P. Ju, J. S. Zhao and C. G. Fu, *Int. J. Electrochem. Sci.*, 12 (2017) 12125.
 15. E. Proietti, F. Jaouen, M. Lefèvre, N. Larouche, J. Tian, J. Herranz and J. P. Dodelet, *Nat. Commun.*, 2 (2011) 416.
 16. R. Silva, D. A. Voiry, M. Chhowalla and T. Asefa, *J. Am. Chem. Soc.*, 135 (2013) 7823.
 17. Y. Deng, Y. Dong, G. Wang, K. Sun, X. Shi, L. Zheng, X. Li and S. Liao, *ACS Appl. Mater. Interfaces*, 9 (2017) 9699.
 18. C. Santoro, A. Serov, R. Gokhale, S. Rojas-Carbonell, L. Stariha, J. Gordon, K. Artyushkova and P. Atanassov, *Appl. Catal. B: Environ.*, 205 (2017) 24.
 19. V. Nallathambi, N. Leonard, S. C. Barton and S. C. Barton, *Electrochem. Solid-State Lett.*, 14 (2011) B55.
 20. S. W. Yuan, J. L. Shui, L. Grabstanowicz, C. Chen, S. Commet, B. Reprögle, T. Xu, L. P. Yu and D. J. Liu, *Angew. Chem. Int. Ed.*, 52 (2013) 8349.
 21. A. Serov, K. Artyushkova and P. Atanassov, *Adv. Energy Mater.*, 4 (2014) 919.
 22. L. Yang, X. F. Zeng, W. C. Wang and D. P. Cao, *Adv. Funct. Mater.*, 28 (2018) 1704537.
 23. X. H. Yan and B. Q. Xu, *J. Mater. Chem. A*, 2 (2014) 8617.
 24. Y. G. Wang, C. L. Zhang, S. F. Kang, B. Li, Y. Q. Wang, L. Q. Wang and X. Li, *J. Mater. Chem.*, 21 (2011) 14420.
 25. G. Wu, C. M. Johnston, N. H. Mack, K. Artyushkova, M. Ferrandon, M. Nelson, J. S. Lezama-Pacheco, S. D. Conradson, K. L. More, D. J. Myers and P. Zelenay, *J. Mater. Chem.*, 21 (2011) 11392.
 26. H. Dong, X. L. Li, Q. Peng, X. Wang, J. P. Chen and Y. D. Li, *Angew. Chem. Int. Ed.*, 44 (2005) 2782.
 27. X. H. Yan, Z. W. Meng, J. Liu and T. Xue, *Mater. Lett.*, 217 (2018) 171.
 28. R. Gokhale, Y. Chen, A. Serov, K. Artyushkova and P. Atanassov, *Electrochem. Comm.*, 72 (2016) 140.
 29. Y. Hu, X. Zhao, Y. J. Huang, Q. F. Li, N. J. Bjerrum, C. P. Liu and W. Xing, *J. Power Sources*, 225 (2013) 129.
 30. J. Zhang, D. P. He, H. Su, X. Chen, M. Pan and S. C. Mu, *J. Mater. Chem. A*, 2 (2014) 1242.
 31. Z. K. Yang, L. Lin and A. W. Xu, *Small*, 12 (2016) 5710.
 32. K. Parvez, S. B. Yang, Y. Hernandez, A. Winter, A. Turchanin, X. L. Feng and K. Müllen, *ACS Nano*, 6 (2012) 9541
 33. Q. Cui, S. J. Chao, P. H. Wang, Z. Y. Bai, H. Y. Yan, K. Wang and L. Yang, *RSC Adv.*, 4 (2014) 12168.
 34. W. Choi, G. Yang, S. L. Kim, P. Liu, H. J. Sue and C. Yu, *J. Power Sources*, 313 (2016) 128.
 35. Z. W. Chang, F. L. Meng, H. X. Zhong and X. B. Zhang, *Chin. J. Chem.*, 36 (2018) 287.
 36. M. Sun, D. Davenport, H. J. Liu, J. H. Qu, M. Elimelech and J. H. Li, *J. Mater. Chem. A*, 6 (2018) 2527.
 37. L. Jiao, G. Wan, R. Zhang, H. Zhou, S. H. Yu and H. L. Jiang, *Angew. Chem. Int. Ed.*, 57 (2018) 8525.
 38. X. Y. Qiu, X. H. Yan, H. Pang, J. C. Wang, D. M. Sun, S. H. Wei, L. Xu and Y. W. Tang, *Adv. Sci.*,

- 6 (2019) 1801103.
39. A. Zitolo, V. Goellner, V. Armel, M. T. Sougrati, T. Mineva, L. Stievano, E. Fonda and F. Jaouen, *Nat. Mater.*, 14 (2015) 937.
40. Y. J. Chen, S. F. Ji, Y. G. Wang, J. C. Dong, W. X. Chen, Z. Li, R. A. Shen, L. R. Zheng, Z. B. Zhuang, D. S. Wang and Y. D. Li, *Angew. Chem. Int. Ed.*, 56 (2017) 6937.
41. A. J. Bard and L. R. Faulkner, *Electrochemical Methods: Fundamentals and Applications*, John Wiley & Sons, (2001) New York, America.
42. W. J. Jiang, L. Gu, L. Li, Y. Zhang, X. Zhang, L. J. Zhang, J. Q. Wang, J. S. Hu, Z. Wei and L. J. Wan, *J. Am. Chem. Soc.*, 138 (2016) 3570.
43. X. X. Yang, X. L. Hu, X. L. Wang, W. Fu, X. Q. He and T. Asefa, *J. Electroanal. Chem.*, 823 (2018) 755.
44. J. H. Kim, Y. J. Sa, H. Y. Jeong and S. H. Joo, *ACS Appl. Mater. Interfaces*, 9 (2017) 9567.
45. Z. Liu, F. Sun, L. Gu, G. Chen, T. T. Shang, J. Liu, Z. Y. Le, X. Y. Li, H. B. Wu and Y. F. Lu, *Adv. Energy Mater.*, 7 (2017) 1701154.

© 2019 The Authors. Published by ESG (www.electrochemsci.org). This article is an open access article distributed under the terms and conditions of the Creative Commons Attribution license (<http://creativecommons.org/licenses/by/4.0/>).